Neuron, Vol. 24, 989–1002, December, 1999, Copyright ©1999 by Cell Press

Supralinear Ca^{2+} Signaling by Cooperative and Mobile Ca^{2+} Buffering in Purkinje Neurons

Hitoshi Maeda,* Graham C. R. Ellis-Davies,† Koichi Ito,* Yasushi Miyashita,*‡ and Haruo Kasai*‡§

*Department of Physiology
Faculty of Medicine
University of Tokyo
Hongo, Bunkyo-ku
Tokyo 113
Japan

†Department of Pharmacology and Physiology
MCP Hahnemann University
Philadelphia, Pennsylvania 19129

‡National Institute for Physiological Sciences
Myodaiji, Okazaki 444
Japan

Summary

Endogenous high-affinity Ca^{2+} buffering and its roles were investigated in mouse cerebellar Purkinje cells with the use of a low-affinity Ca^{2+} indicator and a high-affinity caged Ca^{2+} compound. Increases in the cytosolic Ca^{2+} concentration ($[Ca^{2+}]_i$) were markedly facilitated during repetitive depolarization, resulting in the generation of steep micromolar Ca^{2+} gradients along dendrites. Such supralinear Ca^{2+} responses were attributed to the saturation of a large concentration (0.36 mM) of a mobile, high-affinity (dissociation constant, 0.37 μM) Ca^{2+} buffer with cooperative Ca^{2+} binding sites, resembling calbindin-D_{28K}, and to an immobile, low-affinity Ca^{2+} buffer. These data suggest that the high-affinity Ca^{2+} buffer operates as the neuronal computational element that enables efficient coincidence detection of the Ca^{2+} signal and that facilitates spatiotemporal integration of the Ca^{2+} signal at submicromolar $[Ca^{2+}]_i$.

Introduction

Cytosolic Ca^{2+} regulates many key processes in neurons, and its buffering and diffusion therefore have marked effects on neuronal information processing (Neher, 1998). Many neuronal cells contain large concentrations of relatively fixed Ca^{2+} buffers (Tatsumi and Katayama, 1993; Tse et al., 1994; Kobayashi and Tachibana, 1995; Helmchen et al., 1996); for example, adrenal chromaffin cells contain fixed, low-affinity (dissociation constant, 100 μM) Ca^{2+} binding sites at a concentration of ~4 mM (Xu et al., 1997). Such fixed buffers restrict the apparent diffusion of Ca^{2+}, with the result that Ca^{2+} acts as a short-range messenger (Allbritton et al., 1992; Kasai and Petersen, 1994). In addition, certain populations of neurons contain mobile and high-affinity Ca^{2+} binding proteins (Baimbridge et al., 1992; Heizmann and Braun, 1992). For example, cerebellar Purkinje cells contain large concentrations of the Ca^{2+} binding proteins calbindin-D_{28K} and parvalbumin. Such proteins may play a computational role in central neurons, given that mice deficient in calbindin-D_{28K} exhibit cerebellar ataxia (Airaksinen et al., 1997a) and impaired spatial learning (Molinari et al., 1996). However, the properties of high-affinity Ca^{2+} buffering in vivo and its specific consequences for neuronal Ca^{2+} signaling have not been elucidated.

We have therefore now investigated Ca^{2+} buffering in Purkinje cells with the use of a low-affinity (~10 μM) Ca^{2+} indicator dye (BTC) and a high-affinity (19 nM) caged Ca^{2+} compound (DMNPE-4). Neither of these compounds interfered to a substantial extent with the intrinsic Ca^{2+}-buffering properties of these cells. We detected the existence of a large concentration of a high-affinity, cooperative, and mobile Ca^{2+} buffer, the properties of which resemble those of calbindin-D_{28K}. We also demonstrated the presence of a fixed, low-affinity Ca^{2+} buffer with a binding ratio of ~100. Demonstration of the existence of two Ca^{2+} buffers with markedly different Ca^{2+} binding properties allowed the diffusion of Ca^{2+} to be described by a nonlinear cable equation, which predicts two-phase Ca^{2+} dynamics. Such dynamics may contribute to various computational processes in neurons, including coincidence detection mechanisms of Hebbian learning. Some of the present data were presented in preliminary form (H. Maeda et al., 1998, Soc. Neurosci., abstract).

Results

Supralinear Ca^{2+} Responses in Cerebellar Purkinje Cells

Figure 1A shows a cultured Purkinje cell that was clamped in the whole-cell mode at −70 mV and then depolarized to 0 mV for 0.5 s. Ratiometric measurement of the cytosolic free Ca^{2+} concentration ($[Ca^{2+}]_i$) with the low-affinity Ca^{2+} indicator benzothiazole coumarin (BTC) revealed that the depolarization-induced increase in $[Ca^{2+}]_i$ was sigmoidal, or occurred in two phases; it was slow initially and then markedly accelerated during the depolarization command (Figures 1A and 1B), with an apparent threshold at ~1 μM. The $[Ca^{2+}]_i$ in the dendrites subsequently returned to control values more rapidly than did that in the soma (Figure 1C). The recovery of $[Ca^{2+}]_i$ also occurred with a double-exponential time course, or in two phases, characterized by time constants of 2 to 3 s at $[Ca^{2+}]_i$ of >1 μM (Figure 1C) and of 30 to 40 s at $[Ca^{2+}]_i$ of <1 μM. Thus, changes in $[Ca^{2+}]_i$ appeared to be hindered at a Ca^{2+} concentration of ~1 μM during both the depolarization-induced increase and subsequent decrease in $[Ca^{2+}]_i$. The $[Ca^{2+}]_i$ achieved at the end of the depolarization pulse was highly variable among different parts of the cell; however, in most instances, it was greater in the dendrites [range, 10 to 200 μM; mean ± SD, 30 ± 20 μM (n = 9)] than in the

§To whom correspondence should be addressed (e-mail: hkasai@nips.ac.jp).

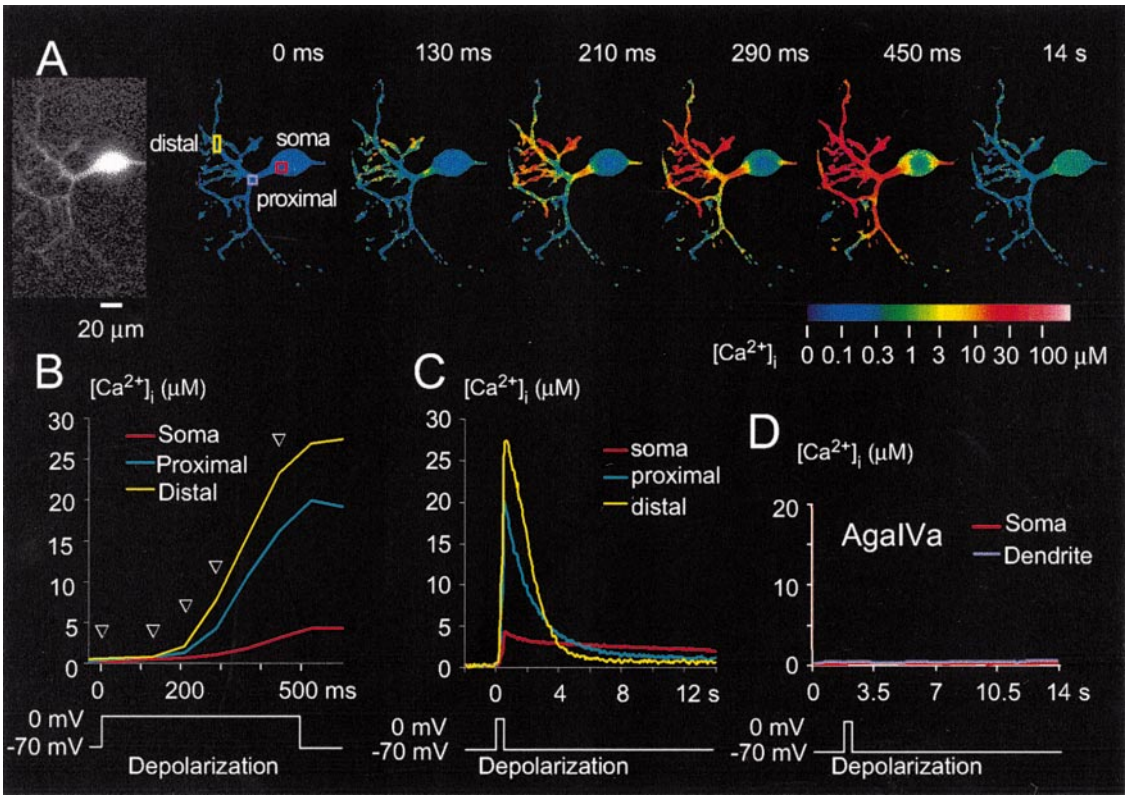

Figure 1. Two-Phase Responses of $[Ca^{2+}]_i$ Induced by a Prolonged Depolarization Command in Cultured Purkinje Neurons

(A) Pseudocolor images of the increases in $[Ca^{2+}]_i$ induced by a 500 ms depolarization command. The Ca^{2+} images were generated from the fluorescence ratio of BTC. The image denoted by 0 ms was acquired immediately before depolarization, and those denoted by 130, 210, 290, and 450 ms were obtained during depolarization. The black-and-white photograph is a fluorescence image of the cell excited at a wavelength of 480 nm.

(B) Time courses of $[Ca^{2+}]_i$ during depolarization that were obtained at the three different regions of the cell indicated in (A): the soma as well as proximal and distal dendrites. Open triangles indicate the time points at which the Ca^{2+} images shown in (A) were acquired.

(C) Time courses of $[Ca^{2+}]_i$ recovery during and after depolarization at the same three regions of the cell as those in (B).

(D) Prevention of the depolarization-induced increase in $[Ca^{2+}]_i$ by AgaIVa. A Purkinje cell different from that in (A) through (C) was pretreated with 100 nM AgaIVa for 2 min before depolarization.

soma (1 to 13 μM; 5 ± 3 μM). The increases in $[Ca^{2+}]_i$ were eliminated by treatment of cells with AgaIVa, a blocker of voltage-gated Ca^{2+} channels, at a concentration of 100 nM (Figure 1D) (Mintz et al., 1992).

Similar two-phase onsets of $[Ca^{2+}]_i$ increases were also observed when a train of short-duration (50 ms) depolarization commands was applied to Purkinje cells at a frequency of 1 Hz (Figure 2). The increment in $[Ca^{2+}]_i$ ($\Delta[Ca^{2+}]_i$) induced by each depolarization pulse was initially small and then increased with the number of pulses (Figures 2B and 2C). The time course of this facilitation varied greatly among different dendritic branches (Figures 2A and 2C), but it always developed slowly in the soma. However, facilitation of $\Delta[Ca^{2+}]_i$ gradually increased in all regions of the cell after the initial $[Ca^{2+}]_i$ ($[Ca^{2+}]_{i,0}$) exceeded 0.4 μM (Figure 2D). Thus, it appeared that the more-than-additive, or supralinear, increases in $[Ca^{2+}]_i$ were triggered after a threshold $[Ca^{2+}]_i$ was achieved. Similar supralinear increases in $[Ca^{2+}]_i$ were induced either by 10 ms depolarization commands applied at 4 Hz ($n = 6$) or when a K^+-based intracellular solution was used instead of the usual Cs^+-based one ($n = 5$) (data not shown).

The supralinear $[Ca^{2+}]_i$ responses were also detected with the high-affinity Ca^{2+} indicator fura-2 (Figure 3). Sigmoidal increases in $[Ca^{2+}]_i$ were induced during a long-duration (0.5 s) depolarization command applied at the soma (Figure 3A). The recovery of $[Ca^{2+}]_i$ also occurred with two exponential components characterized by time constants of 3 s (Figure 3B) and 20 to 40 s, respectively. Facilitation of $\Delta[Ca^{2+}]_i$ was apparent in all regions of the cell in response to repetitive depolarization (Figures 3C and 3D). Similar observations have been described with slice preparations, in which fura-2 was used to monitor Ca^{2+} signals in Purkinje cells in response to either repetitive depolarization (Miyakawa et al., 1992; Llano et al., 1994) or repetitive stimulation of climbing fibers (Miyakawa et al., 1992). The supralinear responses observed with fura-2 were less pronounced than were those measured with BTC; thus, the sigmoidal onset was only barely detected in the soma (Figure 3A), and facilitation during repetitive pulses was apparent only after four or five successive pulses (Figure 3C). In addition, the increases in fura-2 fluorescence ratio did not differ substantially among the soma and dendrites (Figures 3A and 3C). These observations are readily

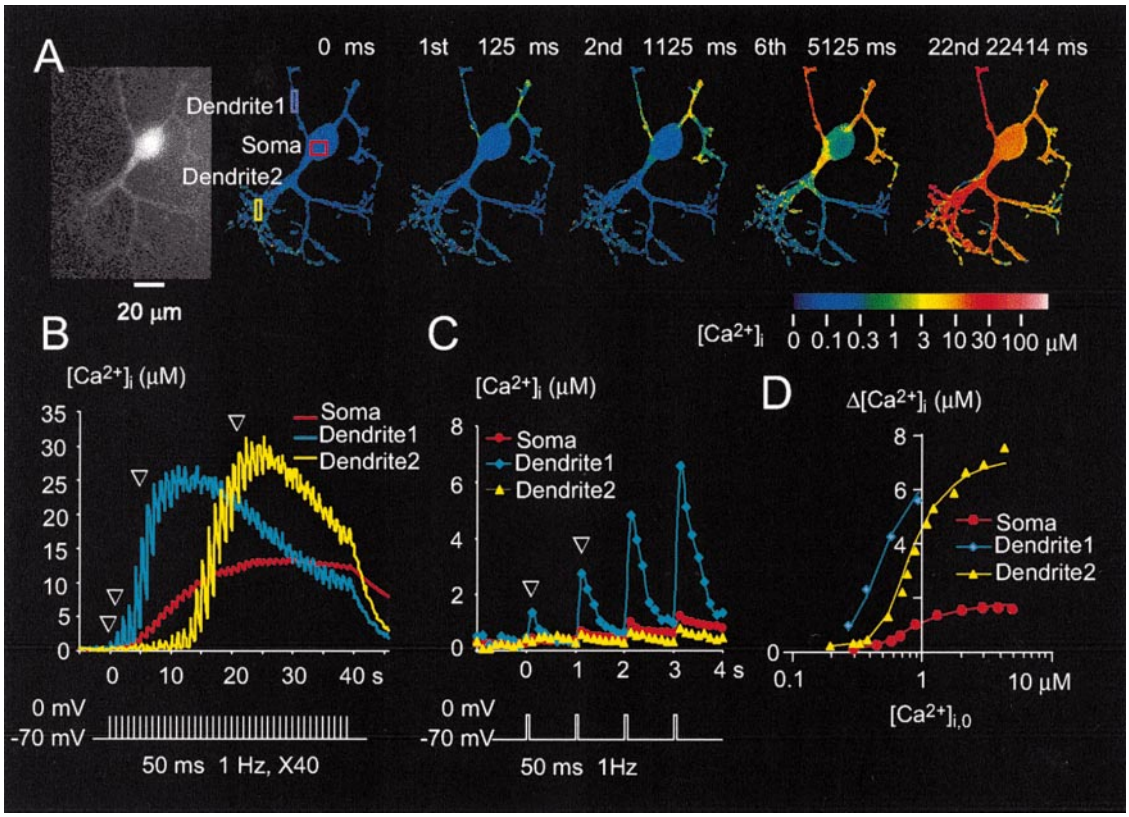

Figure 2. Supralinear Summation of $[Ca^{2+}]_i$ Increases Induced by Repetitive, Short-Duration Pulses of Depolarization

(A) Pseudocolor images of $[Ca^{2+}]_i$ increases induced by a train of 50 ms depolarization commands at a frequency of 1 Hz. The Ca^{2+} images were generated from the fluorescence ratio of BTC and were obtained before depolarization (0 ms) and immediately after the 1st, 2nd, 6th, and 22nd depolarization commands. The black-and-white photograph is a fluorescence image of the cell.

(B) Time courses of $[Ca^{2+}]_i$ during repetitive depolarization obtained at the three different regions of the cell indicated in (A): soma, dendrite 1, and dendrite 2.

(C) Time courses of $[Ca^{2+}]_i$ increases induced by the first four depolarization commands. Open triangles in (B) and (C) indicate the time points at which the Ca^{2+} images shown in (A) were acquired.

(D) Dependence of the increment in $[Ca^{2+}]_i$ ($\Delta[Ca^{2+}]_i$) on the initial $[Ca^{2+}]_i$ ($[Ca^{2+}]_{i,0}$) at the time of depolarization.

explained by the saturation of fura-2 as a result of the large increases in $[Ca^{2+}]_i$ (Figures 9A and 9B) revealed by imaging with BTC (Figures 1 and 2). Correct estimation of $[Ca^{2+}]_i$ from such data requires precise evaluation of R_{max} in vivo, which is practically impossible because of cell-to-cell variability and subcellular heterogeneity of this parameter (Kasai and Takahashi, 1999).

Origin of Supralinear Ca^{2+} Responses

It was possible that the supralinearity of the observed Ca^{2+} responses was due to facilitation of Ca^{2+} influx (Miyakawa et al., 1992). Figure 4A shows the peak amplitudes of inward currents corresponding to Ca^{2+} influx induced by two consecutive 50 ms depolarization pulses (Hirano and Ohmori, 1986). The peak amplitude of the Ca^{2+} currents remained relatively constant during repetitive depolarization (Figures 4A and 4B) ($n = 5$), whereas marked facilitation of the Ca^{2+} responses was apparent in both the soma and dendrites of the same cell (Figures 4C and 4D).

We next investigated whether Ca^{2+} release from intracellular stores was required for the supralinear Ca^{2+} responses (Llano et al., 1994; Hashimoto et al., 1996). To eliminate the effects of Ca^{2+} release from intracellular stores, we used cyclopiazonic acid (CPA) (Fierro et al., 1998). Caffeine induced reproducible increases in $[Ca^{2+}]_i$ after stimulation of Purkinje cells with high concentrations of K^+ (Figure 4E), as previously demonstrated (Kano et al., 1995). However, depletion of intracellular Ca^{2+} stores by CPA prevented such caffeine-induced increases in $[Ca^{2+}]_i$ (Figure 4F). In contrast, CPA did not affect the supralinear Ca^{2+} responses to depolarization (Figure 4G) or the dependence of facilitation on $[Ca^{2+}]_{i,0}$ (Figure 4H). The supralinear Ca^{2+} responses were apparent even when ruthenium red (20 μM) was present in the patch pipette to block Ca^{2+}-induced Ca^{2+} release (Figure 4G, $n = 5$) (Llano et al., 1994). Finally, we seldom observed a clear delay in $[Ca^{2+}]_i$ increases after depolarization, which is a characteristic of Ca^{2+}-induced Ca^{2+} release (Llano et al., 1994); a small delay sometimes apparent in such $[Ca^{2+}]_i$ increases (soma of figures 3B, 3C, and 5E) could be attributed to the diffusion of Ca^{2+} from dendritic branches, in which the induced $[Ca^{2+}]_i$ increases were larger (Figures 1 and 2). Thus, neither modulation of Ca^{2+} influx nor Ca^{2+} release from intracellular stores was the major source for the supralinearity

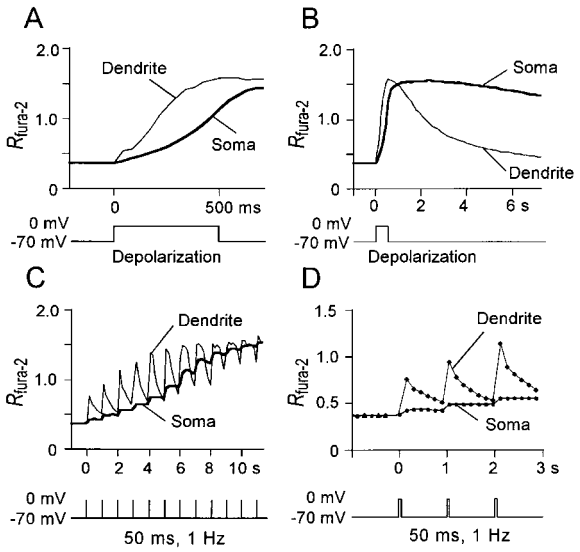

Figure 3. Two-Phase Responses of Fura-2 Fluorescence to Depolarization in Purkinje Cells

(A) Increases in the fluorescence ratio (R_{fura-2}) of fura-2 in the soma and a dendrite of a Purkinje cell during a 500 ms depolarization command.

(B) Time courses of $[Ca^{2+}]_i$ recovery after the 500 ms depolarization pulse for the cell studied in (A).

(C) Time courses of $[Ca^{2+}]_i$ in the soma and a dendrite of a Purkinje cell during repetitive 50 ms depolarization pulses applied at a frequency of 1 Hz.

(D) Time courses of the $[Ca^{2+}]_i$ increases induced by the first three depolarization commands for the cell studied in (C).

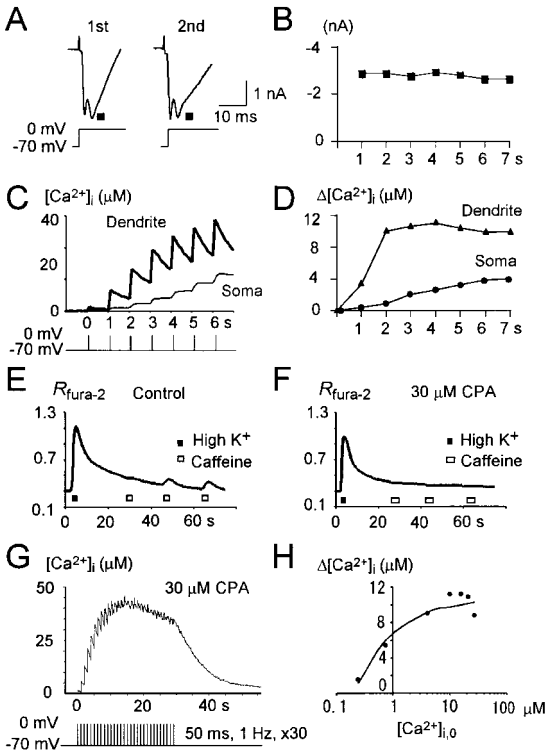

Figure 4. Role of Ca^{2+} Influx and Ca^{2+} Release from Intracellular Stores in the Supralinear Ca^{2+} Responses of Purkinje Cells to Depolarization

(A) Inward currents mediated by Na^+ and Ca^{2+} channels during repetitive stimulation with 50 ms depolarization commands at a frequency of 1 Hz. Closed squares indicate the second peak of inward current, which was resistant to the Na^+ channel blocker tetrodotoxin and corresponds to Ca^{2+} influx.

(B) Peak amplitudes of the Ca^{2+} currents plotted against time.

(C and D) Changes in $[Ca^{2+}]_i$ (C) and $\Delta[Ca^{2+}]_i$ (D) measured from BTC fluorescence in the soma and a dendrite of the same cell as that in (A) and (B).

(E and F) Inhibition of caffeine-induced Ca^{2+} release by CPA. A fura-2-loaded cell was stimulated with 100 mM KCl (closed squares) and 20 mM caffeine (open squares) in the absence (E) or presence (F) of 30 μM CPA. Fura-2 fluorescence was measured from a dendrite.

(G and H) Supralinear Ca^{2+} response to repetitive depolarization (G) and dependence of $\Delta[Ca^{2+}]_i$ on $[Ca^{2+}]_{i,0}$ in the dendrite of a cell loaded with BTC and ruthenium red (20 μM) and exposed to 30 μM CPA.

in the Ca^{2+} responses of cultured Purkinje cells, suggesting that Ca^{2+}-buffering mechanisms might underlie this phenomenon.

Supralinear Ca^{2+} Responses Induced by a Caged Ca^{2+} Compound

We next determined whether supralinear Ca^{2+} responses were evoked by photolysis of a high-affinity caged Ca^{2+} compound, DMNPE-4 (Ellis-Davies, 1998). The dissociation constants for the caged and photolysed forms of DMNPE-4 are 19 nM and 300 μM, respectively, at pH 7.4 (DelPrincipe et al., 1999), so that neither form of the compound substantially affects Ca^{2+} buffering in the physiological range of $[Ca^{2+}]_i$ between 0.3 and 10 μM. Purkinje cells were perfused intracellularly for 5 min with DMNPE-4 (5 mM) saturated with Ca^{2+} and were then subjected to repetitive light pulses to induce photolysis of 6% of the caged Ca^{2+} compound per pulse throughout the cell. We mostly studied the somatic region of cells, where the concentrations of the components of the internal solution can be optimally controlled and where the fluorescence of BTC was greatest (Figures 1 and 2). The repetitive photolysis induced increases in $[Ca^{2+}]_i$ that were facilitated (Figure 5A) in a manner similar to that of the facilitation of the $[Ca^{2+}]_i$ increases induced by repetitive depolarization (Figure 5E) in the same cell. The relation between $\Delta[Ca^{2+}]_i$ (ΔC) and $[Ca^{2+}]_{i,0}$ (C_0) for repetitive photolysis (Figure 5B) was similar to that for repetitive depolarization (Figure 5F). These observations suggested that a high-affinity Ca^{2+} buffer might be responsible for the supralinearity of the Ca^{2+} responses to depolarization. The presence of such a Ca^{2+} buffer could also explain the double-exponential decay in $[Ca^{2+}]_i$ observed after a prolonged depolarization command (Figures 1C and 3B) (Fierro et al., 1998).

Such buffering effects must occur rapidly, because we were not able to detect the Ca^{2+} equilibration process that could account for the supralinearity (Figures 2C, 3D, 4C, 5A, and 5E); the equilibration thus likely took place within the image acquisition time of 80 to 140 ms. These kinetic properties also exclude a role for slower Ca^{2+}-clearing processes, such as Ca^{2+} removal by pumps in the plasma membrane or in the endoplasmic reticulum or by uptake into mitochondria (Xu et al., 1997).

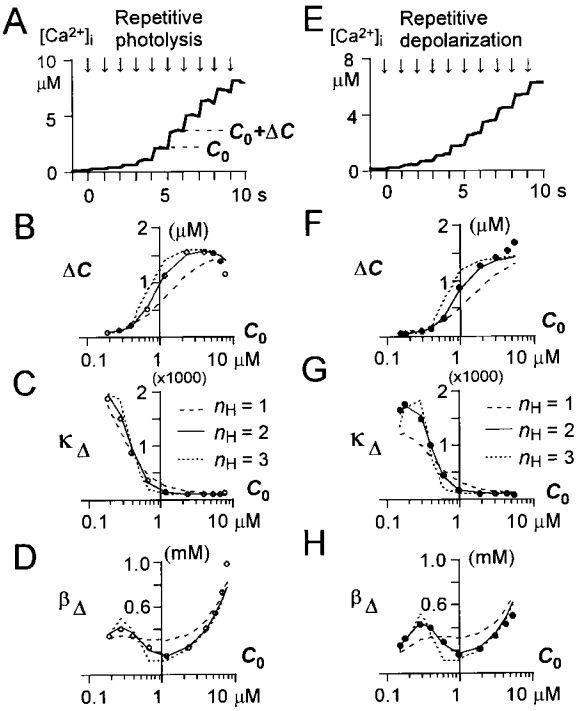

Figure 5. The Ca^{2+} Binding Ratio and Buffering Capacity for a Purkinje Cell Determined by Repetitive Photolysis of Caged Ca^{2+} or Repetitive Depolarization

(A and E) Time courses of $[Ca^{2+}]_i$ increases induced by either repetitive partial (6%) photolysis of the caged Ca^{2+} compound DMNPE-4 (A) or repetitive 50 ms pulses of depolarization (E) in the same BTC-loaded cell. Arrows indicate the timing of photolysis or depolarization.

(B and F) Dependence of $\Delta[Ca^{2+}]_i$ (ΔC) on the $[Ca^{2+}]_{i,0}$ (C_0) immediately before photolysis (B) or depolarization (F). The values for C and C_0 were obtained as indicated in (A).

(C and G) Ca^{2+} dependence of the Ca^{2+} binding ratio (κ_Δ) obtained with the use of Equation 10 (see the Experimental Procedures) for repetitive photolysis (C) or depolarization (G).

(D and H) Ca^{2+} dependence of the Ca^{2+}-buffering capacity (β_Δ) obtained from Equation 11 for repetitive photolysis (D) or depolarization (H).

The polygonal lines in (B) through (D) and (F) through (H) indicate analytical fits of the data with Equations 18 and 19, assuming n_H values of 1, 2, or 3.

Quantitative analysis of our data (Figures 5D and 6) ($n = 9$), as described in the Discussion, predicts the existence of a large concentration (0.36 mM) of a high-affinity (macroscopic dissociation constant, 0.37 μM) and cooperative Ca^{2+} buffer with a Hill coefficient (n_H) of 2 as well as the presence of a low-affinity Ca^{2+} buffer with a Ca^{2+} binding ratio of ~100 (Table 1). The Ca^{2+} binding ratio (κ) obtained with our approach was in the range of 1200 to 2000 at a $[Ca^{2+}]_i$ of 0.2 μM (Figure 5C), consistent with a previous estimation obtained for Purkinje cells in slice preparations (Fierro and Llano, 1996). A similar concentration of the high-affinity Ca^{2+} buffer appears to be present in dendrites, because similar values of [*H*] were obtained from proximal dendrites when we assumed the concentration of DMNPE-4 to be diluted by a factor of 0.7 to 0.2, as was that of BTC (data not shown).

To further assess our methodology, we applied the same experimental protocol to bovine adrenal chromaffin cells, in which Ca^{2+} buffering has been well characterized (Neher and Augustine, 1992; Xu et al., 1997) and the depolarization-induced Ca^{2+} response does not exhibit supralinearity (Neher and Augustine, 1992). As expected, repetitive photolysis of DMNPE-4 resulted in an approximately linear increase in $[Ca^{2+}]_i$ (Figure 7A), indicating the absence of high-affinity Ca^{2+} buffering. Quantitative analysis of our data predicted the presence of a low-affinity Ca^{2+} buffer with a binding ratio of 40 (Figures 7B–7D) ($n = 5$), consistent with previous results (Neher and Augustine, 1992). Moreover, when we added the Ca^{2+} chelator 5,5′-difluoro-BAPTA (dissociation constant, 0.65 μM) at a concentration of 1 mM to the internal solution, repetitive photolysis of DMNPE-4 resulted in a supralinear Ca^{2+} response (Figure 7E) ($n = 4$) similar to that observed in cerebellar Purkinje cells in the absence of the Ca^{2+} chelator (Figure 5A). Quantitative analysis yielded estimates of the dissociation constant and concentration of the Ca^{2+} chelator of 0.6 μM and 1 mM, respectively, with little cooperativity in Ca^{2+} binding (Figure 7H; see the Experimental Procedures). These results thus validate our approach for studying endogenous Ca^{2+} buffers in Purkinje cells. In particular, they confirm the positive cooperativity of the high-affinity Ca^{2+} buffering in these cells.

Mobility of Ca^{2+} Buffers in the Soma

Steep Ca^{2+} gradients were apparent at high $[Ca^{2+}]_i$ in Purkinje cells subjected to depolarization (Figures 1A and 2A), suggesting that the mobility of Ca^{2+} was restricted at high $[Ca^{2+}]_i$. To estimate the diffusion coefficients of the two Ca^{2+} buffers, we investigated the spread of Ca^{2+} in the somatic region of the cell; control of the membrane potential by whole-cell clamping is optimal and the pump rate is low (~5/s) (see the Discussion) in the soma, and possible gradients of pumps in the soma make a negligible contribution to the equilibration of $[Ca^{2+}]_i$. We analyzed the equilibration of $[Ca^{2+}]_i$ after the cessation of depolarization (and of the associated Ca^{2+} influx), so that it should mostly reflect Ca^{2+} diffusion. We chose to study those cells with a bipolar morphology in which increases in $[Ca^{2+}]_i$ occurred predominantly at both poles of the soma (Figure 1A) and Ca^{2+} diffusion occurred mostly in parallel to the main somatic axis.

The rate of spread of Ca^{2+} was greater at submicromolar $[Ca^{2+}]_i$ than at micromolar $[Ca^{2+}]_i$ (Figure 8) ($n = 6$). Depolarization for 50 ms resulted in a peak $[Ca^{2+}]_i$ of 0.7 μM in the outermost compartment of the soma, and equilibration of the Ca^{2+} gradient occurred with a time constant of 0.2 to 0.3 s (Figure 8A). Similar values were obtained in a slice preparation (Eilers et al., 1995b). In contrast, depolarization of the same cell for 500 ms resulted in a peak $[Ca^{2+}]_i$ of 12 μM, and equilibration occurred with a time constant of 1 s (Figure 8B). These data provided estimates for the diffusion constants of the high-affinity (D_H) and low-affinity (D_L) Ca^{2+} buffers of 80 ± 15 $\mu m^2/s$ (mean ± SD, $n = 6$) and <15 $\mu m^2/s$ ($n = 6$), respectively (Figure 8; see the Discussion and Experimental Procedures).

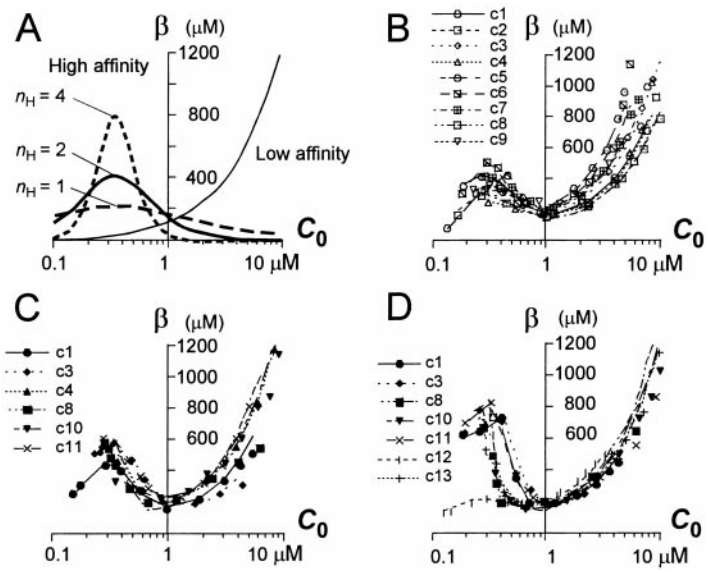

Figure 6. The Ca^{2+}-Buffering Capacity of Purkinje Cells

(A) Theoretical Ca^{2+} dependence of the buffering capacity of high-affinity (n_H = 1, 2, or 4) and low-affinity Ca^{2+} buffers. The concentration of the high-affinity Ca^{2+} buffer, [*H*], is $0.8/n_H$ mM, and the binding ratio of the low-affinity buffer is 100.

(B) Actual buffering capacity obtained from data for DMNPE-4 photolysis in nine Purkinje cells. Plots were obtained by the slope method (Equation 11). Polygonal lines represent the best fit of the data with the analytical method (Equation 19). The data shown in Figure 5 are from the cell c1.

(C and D) Ca^{2+} dependence of the buffering capacity in the soma (C) and in the dendrites (D) of Purkinje cells as determined from experiments based on repetitive depolarization. The data points were obtained by first estimating the constant Ca^{2+} influx by the analytical method to fulfill either the [*H*] acquired in the repetitive photolysis experiments (c1, c3, c4, c8) or β_Δ = 200 μM at C = 1 μM (c10, c11, c12, c13); the plot of β_Δ was then derived from Equations 16 and 11 after determination of ΔC_T.

Discussion

We have detected a large concentration of a high-affinity Ca^{2+} buffer in cerebellar Purkinje cells, the presence of which gives rise to supralinear and micromolar Ca^{2+} responses and their double-exponential decay (Figure 9A). Although the high-affinity Ca^{2+} indicator fura-2 is able to detect these phenomena, it does so in a distorted manner as a result of saturation (Figure 9B).

Ca^{2+} Buffering in Purkinje Cells

To characterize the properties of the high-affinity Ca^{2+} buffer in Purkinje cells, we first attempted to estimate the Ca^{2+} dependence of the Ca^{2+}-buffering capacity defined by Equation 2 (see the Experimental Procedures) with the use of the data obtained by repetitive photolysis of DMNPE-4 (Figure 5). The buffering capacity can be either approximated by the slope method based on Equation 11 (Figure 6A; symbols in Figure 6B) or derived analytically by assuming the presence of high- and low-affinity Ca^{2+} buffers (Equation 17) (polygonal lines in Figure 6B; Table 1). For simplicity, we assume full cooperativity for the Ca^{2+} binding sites of the high-affinity Ca^{2+} buffer (Equation 3). Both methods consistently predicted the existence of high- and low-affinity Ca^{2+} buffers with the properties depicted in Figure 6 and Table 1.

The Ca^{2+} dependence of the buffering capacity can also be obtained from the repetitive depolarization experiments, if we assume a constant Ca^{2+} influx (ΔC_T) at each depolarization. Such plots obtained for the soma (Figures 5H and 6C) and dendrites (Figure 6D) were similar to those obtained from the repetitive photolysis experiments. Thus, the supralinear Ca^{2+} responses in the soma and dendrites appear to be attributable predominantly to saturation of the high-affinity Ca^{2+} buffer, although we cannot rule out a possible role for Ca^{2+} release mechanisms (Llano et al., 1994; Hashimoto et al., 1996).

Table 1. Parameters of Ca^{2+} Buffers in the Soma of Purkinje Neurons

Cell Number	K_H (μM)	n_H	[*H*] (μM)	κ_L
c1	0.35	2	370	100
c2	0.45	2	330	85
c3	0.3	2	380	120
c4	0.4	2	330	125
c5	0.47	4	133	180
c6	0.39	3	280	160
c7	0.35	2	470	130
c8	0.37	2	360	85
c9	0.35	2	390	135
Mean	0.37	2.3	361[a]	130
SD	0.05		51[a]	27

K_H, n_H, and [*H*] represent the macroscopic dissociation constant, Hill coefficient, and concentration of the high-affinity Ca^{2+} buffer, respectively; κ_L is the Ca^{2+} binding ratio for the low-affinity Ca^{2+} buffer.

[a] Mean and SD values were obtained assuming [*H*] of c5 and c6 to be 264 and 375 μM, respectively.

The Ca^{2+} dependence of the buffering capacity can also be obtained from the repetitive depolarization experiments, if we assume a constant Ca^{2+} influx (ΔC_T) at each depolarization. Such plots obtained for the soma (Figures 5H and 6C) and dendrites (Figure 6D) were similar to those obtained from the repetitive photolysis experiments. Thus, the supralinear Ca^{2+} responses in the soma and dendrites appear to be attributable predominantly to saturation of the high-affinity Ca^{2+} buffer, although we cannot rule out a possible role for Ca^{2+} release mechanisms (Llano et al., 1994; Hashimoto et al., 1996).

Ca^{2+} Channels and Pumps

We detected steep micromolar Ca^{2+} gradients in dendrites during depolarization (Figures 1 and 2), indicating marked heterogeneity in the distribution of Ca^{2+} channels. In addition, the greater surface-to-volume ratio also contributes to the larger size of $[Ca^{2+}]_i$ increases in dendrites compared with those in the soma (Hockberger et al., 1989), because the mean density of Ca^{2+} current was estimated as 1.2 and 1.5 pA/μm^2, respectively, from the analysis shown in Figure 6: the Ca^{2+} influx induced by a 50 ms depolarization corresponds to 400 to 1200 μM [mean ± SD, 820 ± 140 μM (n = 7)] and 80 to 150 μM [110 ± 40 μM (n = 6)] Ca^{2+} in dendrites and the soma, respectively, which have typical diameters of 2 and 20 μm, respectively.

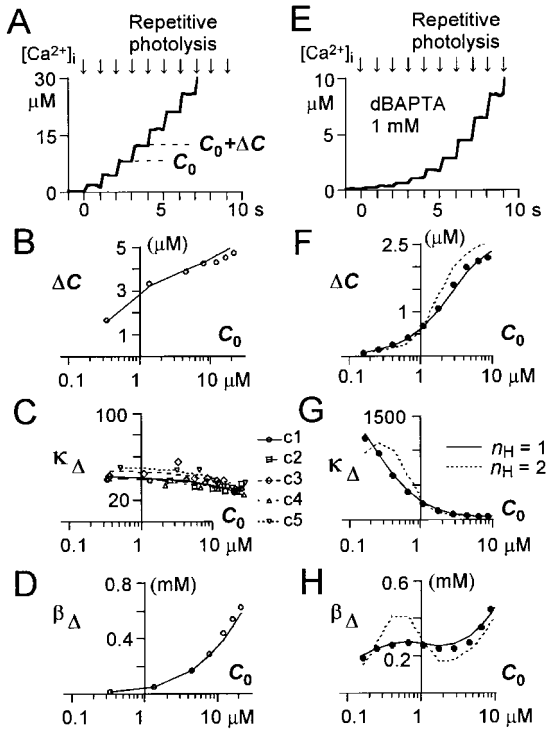

Figure 7. The Ca^{2+} Binding Ratio and Buffering Capacity for Adrenal Chromaffin Cells in the Absence (A–D) or Presence (E–H) of Internal 5,5′-Difluoro-BAPTA

(A and E) Time courses of $[Ca^{2+}]_i$ increases induced by repetitive partial (6%) photolysis of DMNPE-4 in BTC-loaded cells in the absence (A) or presence (E) of intracellular perfusion with 1 mM 5,5′-difluoro-BAPTA (dBAPTA). Arrows indicate the timing of photolysis. (B and F) Dependence of ΔC on the C_0 immediately before photolysis. The values for ΔC and C_0 were obtained as indicated in (A). (C and G) Ca^{2+} dependence of the Ca^{2+} binding ratio (κ_Δ) obtained from Equation 10. Data from five different cells are plotted in (C). (D and H) Ca^{2+} dependence of the Ca^{2+}-buffering capacity (β_Δ) obtained from Equation 11. The polygonal lines in (F) through (H) indicate analytical fits of the data with Equations 18 and 19, assuming an n_H of 1 or 2.

The pump rate also appears to be proportional to the surface-to-volume ratio and likely represents that of the plasma membrane in our cultured cells. If we assume linear pumping activity, P, as defined by Equation 22, the Ca^{2+} responses to repetitive depolarization can be well mimicked by $\Delta C_T = 800$ μM and $P = 50$/s for dendrites and $\Delta C_T = 80$ μM and $P = 5$/s for the soma (Figure 9A). For slice preparations, however, in which Ca^{2+} uptake into intracellular stores appears to play a major role (Fierro et al., 1998), a pump rate about 40 times larger (2000/s) is predicted for the dendrites of Purkinje cells (Airaksinen et al., 1997a) and of cortical pyramidal cells (Helmchen et al., 1996; Markram et al., 1998). Indeed, the decay of Ca^{2+} transients induced by climbing fiber stimulation or depolarization occurred with two time constants of 0.08 and 0.7 s in slice preparations (Miyakawa et al., 1992; Airaksinen et al., 1997a), which are 1/40 of the values obtained with our cultured cells (2 to 3 and 20 to 40 s) (Figures 1C and 3B). The reason for the lesser role of Ca^{2+} clearance mechanisms in cultured Purkinje cells remains to be clarified.

Molecular Identity of the High-Affinity Ca^{2+} Buffer

The high-affinity Ca^{2+} buffer in Purkinje cells is most likely calbindin-D_{28K}, which constitutes 15% of the soluble protein of these cells (Baimbridge et al., 1982; Yamakuni et al., 1987), contains three or four high-affinity (dissociation constant, 0.3 μM) and cooperative binding sites (Cheung et al., 1993) that exhibit rapid binding kinetics, and is thought to be mobile (Roberts, 1993). Indeed, in calbindin-D_{28K} knockout mice, the Ca^{2+} responses of Purkinje cells to climbing fiber stimulation were markedly augmented, and Ca^{2+} recovery occurred with an additional rapid component (time constant, 80 ms) (Airaksinen et al., 1997a). Such a component can be explained by a micromolar increase in $[Ca^{2+}]_i$ and by a pump rate of 2000/s and a binding ratio of the low-affinity Ca^{2+} buffer of 160. Although large amounts of parvalbumin are also present in Purkinje cells (Kosaka et al., 1993), this protein may not account for the high-affinity Ca^{2+} buffering revealed in the present study because it exhibits slow Ca^{2+} binding kinetics, as a result of its high-affinity interaction with Mg^{2+} (detected in vitro) (Falke et al., 1994), and its two Ca^{2+} binding sites are noncooperative (Cheung et al., 1993). However, uncertainty remains about the kinetics of parvalbumin in vivo (Chard et al., 1993), and it is possible that both calbindin-D_{28K} and parvalbumin contribute to the rapid, high-affinity Ca^{2+} buffering in Purkinje cells. Saturable high-affinity Ca^{2+} buffers may also be present in certain molluscan neurons (Baker and Schlaepfer, 1978; Ahmed and Connor, 1988; Muller et al., 1993; Al-Baldawi and Abercrombie, 1995).

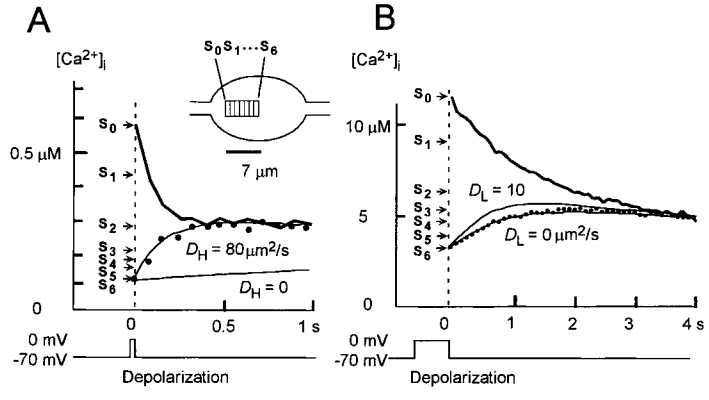

Figure 8. Ca^{2+} Diffusion in the Soma of a Purkinje Cell after Depolarization

Time courses of $[Ca^{2+}]_i$ in the outermost (S_0, thick solid line) and innermost (S_6, closed circles) of seven compartments of the soma ([A], inset) from which averaged $[Ca^{2+}]_i$ values were obtained after a depolarization command of 50 ms (A) or 500 ms (B). The data were obtained from the same cell. Thin lines indicate theoretical prediction of the data, assuming the indicated diffusion coefficients (D) of the Ca^{2+} buffers and the standard buffer parameters. Arrows denoted by S_0,..., S_6 indicate the initial values at the seven compartments. The process of equilibration was not markedly affected by D_L in (A) or by D_H in (B).

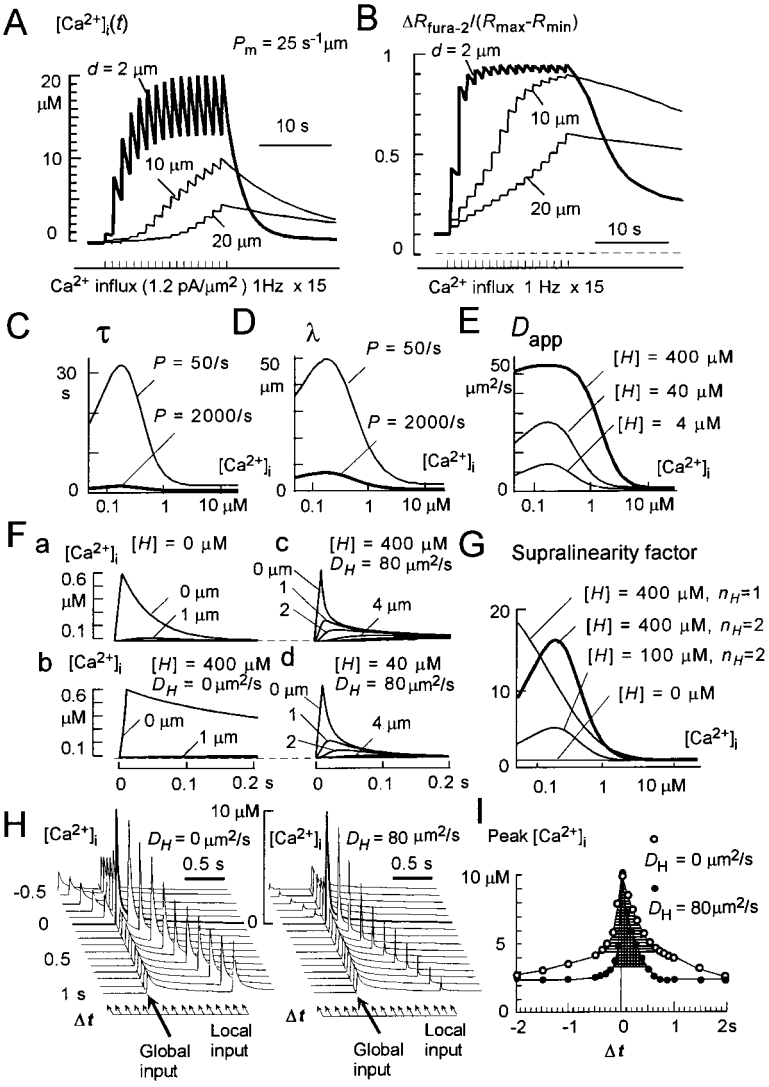

Figure 9. Two-Phase Ca^{2+} Dynamics Predicted by a Nonlinear Cable Equation

(A) Time courses of $[Ca^{2+}]_i$ during repetitive depolarization in cylinders with diameters (d) of 2, 10, or 20 μm, assuming the Ca^{2+} current density as 1.2 pA/μm^2 and the pump rate normalized to the surface-to-volume ratio (P_m) as 25 s^{-1} μm. The resting $[Ca^{2+}]_i$ is 0.1 μM in all simulation experiments in this figure.

(B) Time courses of the fluorescence ratio of fura-2 during the changes in $[Ca^{2+}]_i$ shown in (A). The $K_d\beta$ for fura-2 is set at 0.8 μM.

(C and D) Ca^{2+} dependence of the time constant of Ca^{2+} signaling (t) and the diffusion length of Ca^{2+} (λ), respectively, under conditions of the standard buffer parameters and a pump rate (P) of 50/s or 2000/s.

(E) Ca^{2+} dependence of the apparent diffusion constant (D_{app}) of Ca^{2+} at three different concentrations of the high-affinity buffer ([H]).

(F) Time courses of $[Ca^{2+}]_i$ when Ca^{2+} influx is applied to the middle compartment of a 19-compartment model with a unit length of 1 μm. Concentrations of the high-affinity Ca^{2+} buffer are 0, 400, 400, and 40 μM for (Fa) through (Fd), respectively. The diffusion constant of the high-affinity Ca^{2+} buffer (D_H) is assumed to be 0 μm^2/s for (Fb) and 80 μm^2/s for (Fc) and (Fd). The duration of Ca^{2+} influx is 10 ms, and the total amount was adjusted to achieve a peak $[Ca^{2+}]_i$ of 0.6 μM; the total amounts are 54, 590, 1000, and 155 μM for (Fa) through (Fd), respectively. The distances from the middle compartment are indicated (0 to 4 μm).

(G) Ca^{2+} dependence of the supralinearity factor (S), representing the relative Ca^{2+}-buffering capacity at a certain $[Ca^{2+}]_i$ with respect to that at high $[Ca^{2+}]_i$ (Equation 24).

(H) Supralinear summation of local and global Ca^{2+} inputs applied at various time intervals (Δt) to a 19-compartment model. For the global input (by dendritic Ca^{2+} spike), a Ca^{2+} input of 0.9 mM is applied to all compartments, resulting in an increase in $[Ca^{2+}]_i$ of 2.2 μM. For the local input (synaptic input), a Ca^{2+} input of 1 or 1.1 mM is applied to the middle compartment for a D_H of 0 and 80 μm^2/s, respectively.

(I) Peak amplitudes of $[Ca^{2+}]_i$ when local and global inputs are applied to the 19-compartment model at different time intervals (Δt). The shaded areas represent the time window during which the two successive inputs result in a peak $[Ca^{2+}]_i$ greater than the sum of the individual peak values.

Mobility of Ca^{2+} Buffers

We estimated the diffusion coefficient of the high-affinity Ca^{2+} buffer, D_H, to be 80 μm^2/s (Figure 8A). This diffusion coefficient is consistent with or slightly smaller than values predicted for calbindin-D_{28K} (Roberts, 1993), and it may reflect weak binding of the Ca^{2+} buffer to cellular structures (Heizmann and Braun, 1992). Such a Ca^{2+} buffer would be washed out relatively rapidly (2 min) during whole-cell recording from a cell with a volume of ~1000 μm^3 (Roberts, 1993). In our cells, however, we estimate that the time constant for washout is ~40 min (Push and Neher, 1988), assuming the total volume of the Purkinje cells to be 20,000 μm^3 as a result of the prominent dendritic processes. Given that we completed our analysis within 10 min, we underestimate the amount of Ca^{2+} buffers at most by 23%. Washout of mobile buffers is predicted to be even less of a problem in slice preparations (Fierro and Llano, 1996), given that the volume of Purkinje cells is as large as 800,000 μm^3 in 13-day-old cats (Calvet et al., 1985).

In contrast, the low-affinity Ca^{2+} buffer in Purkinje cells does not appear to be particularly mobile (Figure 8B). The data were best fitted with D_L values of 0 or 15 μm^2/s if the diffusion coefficient of BTC was assumed to be 100 or 0 μm^2/s, respectively. Given that we do not know the precise value of the diffusion coefficient for BTC in our cell preparation, that for the low-affinity Ca^{2+} buffer was estimated to be at most 15 μm^2/s and more likely close to 0 μm^2/s. The low mobility of the low-affinity buffer is consistent with the results of previous studies of Ca^{2+} buffers in adrenal chromaffin cells (Zhou and Neher, 1993) and molluscan neurons (Gabso et al., 1997).

Functional Roles of Neuronal Ca^{2+} Buffers

Our results suggest that high-affinity Ca^{2+} buffering in neurons plays roles in addition to its contribution to neuroprotection (Mattson et al., 1991; Heizmann and Braun, 1992). Thus, mice deficient in calbindin-D_{28K} develop cerebellar ataxia (Airaksinen et al., 1997a) and

show a deficit in spatial memory acquisition (Molinari et al., 1996), even though no gross abnormality or cell death is apparent in the central nervous system (Airaksinen et al., 1997b). Furthermore, Ca^{2+} performs many critical functions in Purkinje cells, including induction of long-term depression (LTD) of the parallel fiber input (Sakurai, 1990; Konnerth et al., 1992) and of long-term potentiation (LTP) of inhibitory postsynaptic currents (Kano et al., 1992), activation of ion channels (Llano et al., 1991; Wang and Augustine, 1995), and modulation of excitability (Hounsgaard and Midtgaard, 1989). These effects of Ca^{2+} are likely profoundly modified by the Ca^{2+}-buffering system.

At $[Ca^{2+}]_i$ in the micromolar range, Ca^{2+} signaling is rapid (Figure 9C) and local (Figures 9D and 9E) as a result of the fixed, low-affinity Ca^{2+} buffer (Kasai and Petersen, 1994). In contrast, at submicromolar $[Ca^{2+}]_i$, the high-affinity Ca^{2+} buffer markedly affects the dynamics of Ca^{2+} signaling. First, the time constant (τ) is greatly increased (Figure 9C), approximately in proportion to the concentration of the high-affinity Ca^{2+} buffer ([*H*]) (Equation 23). Assuming a high pump rate of 2000/s, the corresponding time constant of 0.6 s would allow temporal summation of low-frequency synaptic input, such as climbing fiber stimulation (1 to 4 Hz). Second, the diffusion length (λ) of Ca^{2+} is increased (Figure 9D), approximately in proportion to the square root of [*H*] (Equation 26). The diffusion length of Ca^{2+} (7 μm) in slice preparations (Finch and Augustine, 1998) can be accounted for by a pump rate of 2000/s (Figure 9D). Thus, Ca^{2+} is a diffusible and associative messenger in those neurons with mobile high-affinity buffers, as are molecular second messengers such as inositol trisphosphate (IP_3) and cAMP (Kasai and Petersen, 1994). Third, the apparent diffusion constant (D_{app}) of Ca^{2+} is increased (Figure 9E), approximately in proportion to [*H*] at low [*H*]; the half-maximal value is achieved at an [*H*] of 40 μM, with virtual saturation at 400 μM (Equation 27). The diffusion coefficient reflects Ca^{2+} removal from a focal and transient Ca^{2+} source (Figure 9F): marked spread of Ca^{2+} and hastening of signal decay are induced in the presence of a mobile, high-affinity buffer (Figures 9Fa, 9Fb, and 9Fd) even at a concentration of 40 μM (Figure 9Fd). The large [*H*] present in Purkinje cells facilitates the spread of Ca^{2+} at $[Ca^{2+}]_i$ as large as 1 μM (Figure 9E), which likely contributes to narrowing of the time window for supralinear summation, as discussed below (Figure 9I).

Supralinear and Two-Phase Ca^{2+} Signaling Mediated by Ca^{2+} Buffering

The most pronounced consequence of high-affinity Ca^{2+} buffering in Purkinje cells is the marked supralinearity of Ca^{2+} signaling caused by saturation of the buffer. The effect of buffer saturation can be quantified by the supralinearity factor (*S*) (Equation 24), which represents the efficiency of the high-affinity buffer with respect to that of the low-affinity buffer (Figure 9G). The supralinearity factor increases approximately in proportion to [*H*] and is more steeply dependent on $[Ca^{2+}]_i$ at larger n_H (Figure 9G). A supralinearity factor of 15 at a $[Ca^{2+}]_i$ of 0.2 μM can account for the observed supralinearity of Ca^{2+} responses during repetitive depolarization (Figures 2D and 5E), as well as for the double-exponential decay in $[Ca^{2+}]_i$ (Figures 1C, 3B, and 9A–9C) (Eilers et al., 1995b; Fierro et al., 1998).

The diffusion of the Ca^{2+} buffer further contributes to supralinearity. This effect of diffusion can be illustrated by considering two Ca^{2+} inputs applied at various time intervals, one applied to all compartments (global input, by dendritic spike or climbing fiber stimulation) (Figure 9H) and the other applied to only a middle compartment (local input, by synaptic stimulation). Both inputs are set to induce increases in $[Ca^{2+}]_i$ of 2.2 μM when D_H is assumed to be 0. The supralinear summation of the global and local inputs can be quantified by the peak values of $[Ca^{2+}]_i$ during successive application of the two inputs. Supralinear summation results in a $[Ca^{2+}]_i$ of 10 μM when the two inputs are applied simultaneously, and such summation occurs over a wide temporal window (Figure 9H). The peak $[Ca^{2+}]_i$ is larger than the sum of the peak values for the inputs applied individually when the local input is applied 0.5 s before or 0.7 s after the global input (Figure 9I). In contrast, if we assume the buffer is mobile, with a D_H of 80 $\mu m^2/s$, the summation of the two inputs generates a $[Ca^{2+}]_i$ of 10 μM even though the synaptic Ca^{2+} transient alone is as low as 0.6 μM (Figure 9H), as a result of the rapid spread of Ca^{2+} from the local compartment. Moreover, supralinear summation is induced over a narrower time window; the peak $[Ca^{2+}]_i$ is larger than the sum of the individual peak values when the local input is applied 0.15 s before or 0.45 s after the global input (Figure 9I). Thus, the diffusion of the high-affinity Ca^{2+} buffer increases the extent of supralinearity and narrows the time window for the supralinear summation of Ca^{2+} transients.

Supralinearity of Ca^{2+} responses could provide a mechanism for coincidence detection of two neuronal activities for Hebbian learning; it is postulated that the coincidence of synaptic input to and a postsynaptic spike in the same neuron triggers changes in the synaptic connections that underlie such learning (Linden, 1999). In Purkinje neurons, both complex spikes and parallel fiber input trigger Ca^{2+} mobilization (Tank et al., 1988; Miyakawa et al., 1992; Eilers et al., 1995a; Finch and Augustine, 1998; Takechi et al., 1998). Moreover, the conditions required to induce LTD in various studies are thought to cause micromolar Ca^{2+} responses (Ito et al., 1982; Hirano, 1990; Sakurai, 1990; Linden et al., 1991; Shibuki and Okada, 1991; Konnerth et al., 1992; Hartell, 1996; Lev-Ram et al., 1997; Finch and Augustine, 1998). All of these studies involved repetitive low-frequency stimulation, which, because of the large time constant of the Ca^{2+} signal at low $[Ca^{2+}]_i$ (Figure 9C), effectively results in summation and, in turn, saturation of the high-affinity Ca^{2+} buffer. The time window for LTD induction in vivo (Ekerot and Kano, 1989) is similar to that predicted in Figure 9I (closed circles).

The supralinearity due to the high-affinity Ca^{2+} buffer of Purkinje cells ($S > 15$) would be no less effective than that for two other candidates for coincidence detectors, *N*-methyl-D-aspartate (NMDA)-sensitive glutamate receptors (Sobel and Tank, 1999) and IP_3 receptors (Berridge, 1993; Kasai and Petersen, 1994). The Ca^{2+} permeability of NMDA receptors is increased ~10-fold when the membrane potential is depolarized by 58 mV (Schneggenburger et al., 1993). The Ca^{2+} mobilization mediated by IP_3 receptors increases ~20-fold when $[Ca^{2+}]_i$ increases by a factor of 10 (Kaftan et al., 1997;

Hirose et al., 1998). For optimal supralinearity mediated by NMDA receptors, synaptic input should precede the spike, whereas the opposite is the case for the Ca^{2+} buffer (Figure 9I, closed circles).

In summary, the high-affinity Ca^{2+} buffer confers two-phase dynamics to Ca^{2+} signaling in Purkinje cells: the Ca^{2+} signal is diffusible and slow in the submicromolar phase, whereas it is local and rapid in the micromolar phase. The cooperativity of the Ca^{2+} buffer ensures that neuronal activity is able to promptly trigger the phase transition, which then results in the activation of many downstream events. Nonequilibrium Ca^{2+} dynamics must be more active during the micromolar phase (Kasai, 1993; Markram et al., 1998; Neher, 1998). The performance of the two-phase Ca^{2+} dynamics may be actively maintained, given that increases in $[Ca^{2+}]_i$ upregulate calbindin-D_{28K} expression (Arnold and Heintz, 1997). Thus, our study suggests that two-phase Ca^{2+} dynamics contribute to computational and learning processes in neurons that express high-affinity Ca^{2+} binding proteins.

Experimental Procedures

Cerebellar Cultures

Dispersed cerebellar cultures were prepared from mouse embryos on embryonic day 15 to 18. The dissociated cells were plated at a density of $2.0 \times 10^5/mm^2$ on 15 mm round, glass cover slips that had been coated with 0.05% polyethyleneimine and 0.05% poly-D-lysine (Sigma). The cells were cultured at 37°C in Neurobasal Medium supplemented with 2% B-27 Supplement (GIBCO) and under a humidified atmosphere containing 10% CO_2. The culture medium also contained 5% fetal bovine serum or human serum for the 1st day after plating. The medium was refreshed each week by replacing 20% of the old medium with new medium. Cells cultured for 3 to 5 weeks were used for the electrophysiological experiments. Purkinje cells were readily identified by their prominent dendritic trees; they also exhibited marked calbindin immunoreactivity. Chromaffin cells were isolated from bovine adrenal medulla and cultured as described (Neher and Zucker, 1993; Ninomiya et al., 1997).

Electrophysiology

The cover slips containing the cultured cells were transferred to a recording chamber that was mounted on the stage of an inverted microscope (Olympus IX-70), and the cells were observed with a water-immersion objective lens (60×). The external solution contained 120 mM NaCl, 5 mM KCl, 2 mM $CaCl_2$, 1 mM $MgCl_2$, 10 mM Hepes-NaOH (pH 7.4), and 10 to 30 mM glucose, giving a total osmolarity of 265 mOsm. Tetrodotoxin (Sigma) was present in the extracellular solution at a concentration of 0.5 μM in some experiments. The recording chamber was continuously perfused at a rate of 0.5 to 1 ml/min. The internal solution contained 130 mM cesium gluconate, 10 mM CsCl, 50 mM Hepes-CsOH (pH 7.4), 4 mM ATP (Mg^{2+} salt), and 0.2 mM GTP (Na^+ salt). Cesium was replaced by K^+ in some experiments. Measurement of $[Ca^{2+}]_i$ was performed with the Ca^{2+} indicators BTC or fura-2 (Molecular Probes) at 0.6 and 0.2 mM, respectively. The caged Ca^{2+} compound DMNPE-4 (dimethoxynitrophenyl-EGTA-4) was added to the internal solution at a concentration of 5 mM, and the pH and osmolarity were adjusted to 7.4 and 260 to 280 mOsm, respectively. The DMNPE-4-containing solution was carefully titrated with Ca^{2+} to give a free Ca^{2+} concentration of 0.2 to 0.3 μM. Ruthenium red (20 μM) (Sigma) was added to the internal solution in some experiments. Synthetic ω-AgaIVa (Peptide Institute, Osaka, Japan) and CPA (Sigma) were dissolved in the external solution immediately before use. High (100 mM) K^+ and 20 mM caffeine (Wako, Osaka, Japan) were applied through a glass pipette. In some experiments with adrenal chromaffin cells, 1 mM 5,5′-difluoro-BAPTA (Molecular Probes) was added to the internal solution.

Patch clamp experiments were performed with a patch clamp amplifier (CEZ-2400; Nihon Koden, Tokyo, Japan) and patch pipettes with a resistance of 4 to 7 MΩ; the access resistance was 10 to 30 MΩ (21 ± 4 MΩ, $n = 77$) and was compensated by 40 to 85%. Data were acquired with custom-built software based on LabView 4.0 (National Instruments). All electrophysiological experiments were performed at a room temperature of 24°C to 26°C.

Ca^{2+} Measurement

Calcium imaging was performed with a polychromator and cooled-CCD (charge-coupled device) camera imaging system (T. I. L. L. Photonics, Munich, Germany). Monochromatic beams of light with wavelengths of 340, 380, 430, or 480 nm were isolated from the output of a xenon lamp with the use of the polychromator. The light was reflected by a dichroic mirror (U-MWB and U-MWU for BTC and fura-2, respectively; Olympus) placed beneath the objective lens, and fluorescent light emitted from cells was captured by the cooled-CCD camera system. Fluorescence was excited at 430 and 480 nm for BTC and at 340 and 380 nm for fura-2. The mean duration of light exposure was 8 ms, and the cycle time for acquisition of a pair of images was 80 to 140 ms. The fluorescence ratio was obtained from the pair of images after subtracting the background fluorescence. The calibration parameters ($K_d\beta$, R_{min}, and R_{max}) were obtained from in vivo calibration experiments (Ito et al., 1997), with the use of four calibration solutions in which the free Ca^{2+} concentration was adjusted to 0 μM, 0.1 μM, 10 μM, or 20 mM. Calibration constants for Purkinje cells patch-clamped in the whole-cell mode were as follows: $R_{min} = 0.18$, $R_{max} = 1.7$, and $K_d\beta = 0.8$ μM for fura=2, and $R_{min} = 0.35$, $R_{max} = 1.4$, and $K_d\beta = 67$ μM for BTC. To obtain Ca^{2+} images from BTC fluorescence (Ito et al., 1999), we first estimated the distribution of R_{min} in individual cells by averaging several frames of the resting distribution of R. This procedure was used to compensate for small heterogeneity in R_{min} within a cell and to reduce noise levels, particularly at $[Ca^{2+}]_i$ values of <1 μM. Distributions of ΔR were then calculated by subtracting the distribution of R_{min} from that of R. From ΔR, $[Ca^{2+}]_i$ was estimated as $K_d\beta \times \Delta R/(R_{max} - \Delta R - 0.35)$.

Photolysis of Caged Ca^{2+}

Photolysis of the caged Ca^{2+} compound DMNPE-4 was achieved as described (Ito et al., 1997). In brief, the light from a mercury lamp (IX-RFC; Olympus) was filtered through BP360 and two neutral density filters (ND12 and ND25) (Olympus) and then fed into one port of the light guide. Light was gated through an electric shutter (Copal, Tokyo, Japan), the duration of opening of which was set at 66 ms to activate 6% of DMNPE-4 during each light pulse. For this latter estimation, a small droplet of internal solution (containing 0.1 mM DMNPE-4 and 0.5 mM BTC) formed in mineral oil was subjected to repeated photolysis; the initial photolysis resulted in a change in the fluorescence ratio corresponding to 6% of the total change.

A Nonlinear Theory of Ca^{2+} Buffering and Diffusion

We define the Ca^{2+} binding ratio (κ) (Neher, 1995) and Ca^{2+}-buffering capacity (β) of a solution as

$$\kappa(C) = \frac{dC_B}{dC} \tag{1}$$

$$\beta(C) = \frac{dC_B}{d \ln C} = C \frac{dC_B}{dC} = C\,\kappa(C) \tag{2}$$

where C represents $[Ca^{2+}]_i$ and C_B is the concentration of calcium bound to Ca^{2+} buffers in the solution. A similar quantity, $\beta = (Ca^{2+}$ added$)/d(-pC) = 2.303 \times C \times (\kappa(C)+1)$, was used to represent the Ca^{2+}-buffer capacity conforming to the notion of classical pH buffer capacity (Ahmed and Connor, 1988; Neher, 1995; Schwiening and Thomas, 1996). For simplicity and clarity, however, we use the definition in Equation 2. If the solution contains a buffer with a macroscopic dissociation constant of K_H, a Hill coefficient of n_H, and a concentration of $[H]$, then C_B depends on C as follows

$$C_B = \frac{n_H[H](C / K_H)^{n_H}}{1 + (C / K_H)^{n_H}} \tag{3}$$

and the binding ratio and buffering capacity are given by

$$\kappa_H(C) = \frac{n_H^2[H]C^{n_H-1} / K_H^{n_H}}{(1 + (C / K_H)^{n_H})^2} \quad (4)$$

$$\beta(C) = \frac{n_H^2[H](C / K_H)^{n_H}}{(1 + (C / K_H)^{n_H})^2} \quad (5)$$

The Ca^{2+} dependence of the buffering capacity, $\beta(C)$, allows all parameters of a high-affinity Ca^{2+} buffer to be graphically obtained, given that it takes the maximal value of

$$\beta(K_H) = \frac{n_H^2}{4}[H] \quad (6)$$

at $C = K_H$, and its semilogarithmic plot is a symmetrical distribution whose integral ($\int \beta(C)\, d\ln(C)$) represents the total Ca^{2+} binding sites, $n_H[H]$, and whose slope is steeper at larger n_H (Figure 6A). Indeed, when Ca^{2+} is increased from K_H to $3K_H$, the buffering capacity is reduced by a slope factor (f_s) of

$$f_s = \frac{\beta(K_H)}{\beta(3K_H)} = \frac{(1 + 3^{n_H})^2}{4 \times 3^{n_H}} \quad (7)$$

which is 1.33, 2.77, 7.25, and 20.75 at n_H values of 1, 2, 3, and 4, respectively.

When the solution contains low-affinity ($C << K_H$) and noncooperative Ca^{2+} buffers, the binding ratio (Equation 4) and buffering capacity (Equation 5) are reduced to

$$\kappa(C) = [L]/K_L = \kappa_L \quad (8)$$

$$\beta(C) = \kappa_L \times C \quad (9)$$

Thus, the binding ratio (κ) is constant, κ_L, and the buffering capacity (β) is linearly dependent on C (Figure 6A).

Two approaches can be adopted to obtain buffer parameters from actual data. The first approach (the slope method) relies on the fact that repetitive photolysis of caged Ca^{2+} results in small increments in C; thus, $\Delta C_j = C1_{ij} - C_{0,j}$, at the jth photolysis. For simplicity, we will omit the suffix j whenever possible. The binding ratio (κ_Δ) and buffering capacity (β_Δ) should then be approximated by the difference equations

$$\kappa_\Delta(C_0) = \frac{\Delta C_B}{\Delta C} \quad (10)$$

$$\beta_\Delta(C_0) = C_0 \frac{\Delta C_B}{\Delta C} \quad (11)$$

where ΔC_B is the change in Ca^{2+} concentration bound to the intrinsic Ca^{2+} buffer. In our experiments, C_B is expressed as

$$C_B = C_T - C - C_E \quad (12)$$

where C_T represents the total concentration of cytosolic Ca^{2+}, and C_E represents the concentration of Ca^{2+} bound to extrinsic Ca^{2+} buffers and is described by

$$C_E(C, j) = (1 - a[j]\frac{[DM]\, C / K_{DM}}{1 + C / K_{DM}} + a[j]\frac{[DM]\, C / K_{PDM}}{1 + C / K_{PDM}} + \frac{[BTC]\, C / K_{BTC}}{1 + C / K_{BTC}} \quad (13)$$

$$a[j] = 1 - (1 - b)^j \quad (14)$$

where [*DM*] and [*BTC*] represent total concentrations of DMNPE-4 and BTC in the cell; K_{BTC}, K_{DM}, and K_{PDM} represent the dissociation constants for BTC and caged and photolysed forms of DMNPE-4, and are 15 μM, 19 nM, and 0.3 mM, respectively; and a[j] represents the fraction of DMNPE-4 photolysed by j pulses of radiation, each of which photolyses (100 $\times$ b)% of DMNPE-4. The change in C_E induced by the jth photolysis is now given by

$$\Delta C_E = C_E(C_1, j) - C_E(C_0, j - 1) \quad (15)$$

With this value and assuming $\Delta C_T = 0$, we can estimate ΔC_B from

$$\Delta C_B = \Delta C_T - \Delta C - \Delta C_E \quad (16)$$

The actual plot of β_Δ versus $\ln(C)$ (Figure 6B) indicates the presence of a large concentration (0.3 to 5 mM) of a high-affinity (dissociation constant, 0.3 to 0.4 μM) and cooperative ($n_H = \sim 2$) Ca^{2+} buffer (Figure 6A), as well as a low-affinity Ca^{2+} buffer with a binding ratio of 80 to 150. The Hill coefficient of the high-affinity buffer can be quantified with the use of the slope factor, $f_s = (\beta_\Delta(K_H) - K_H \kappa_L)/(\beta_\Delta(3K_H) - 3K_H\kappa_L)$ (Equation 7), in those cells (c1, c2, c5, c6) that exhibited a clear peak in β_Δ. The slope factors in these cells were 4.16, 4.53, 20.8, and 9.55, which give Hill coefficients of 2.53, 2.52, 4.02, and 3.26, respectively. In contrast, three chromaffin cells loaded with 1 mM 5,5′-difluoro-BAPTA showed slope factors (f_s) of 1.3 (Figure 7H), 1.36, and 1.25, corresponding to Hill coefficients of 0.95, 1.04, and 0.88, respectively.

The second method for obtaining buffer parameters assumes the presence of two Ca^{2+} buffers,

$$C_B(C) = \frac{n_H[H](C / K_H)^{n_H}}{1 + (C / K_H)^{n_H}} + \kappa_L C \quad (17)$$

and the buffer parameters are derived analytically by best fitting. Combining Equations 15 to 17, we obtain the following implicit equation for C_0 and C_1

$$C_B(C_1) - C_B(C_0) = \Delta C_T - (C_1 - C_0) - (C_E(C_1, j) - C_E(C_0, j - 1)) \quad (18)$$

We can predict C_1 from the actual value of C_0 at the jth photolysis by solving Equation 18. With C_0 and the predicted value of C_1, we can obtain β_Δ from

$$\beta_\Delta(C_0) = C_0 \frac{(C_B(C_1) - C_B(C_0))}{(C_1 - C_0)} \quad (19)$$

We then find values for K_H, [H], n_H, and κ_L that minimize the differences between the predicted β_Δ and the actual $\beta\Delta$ at several iterations of partial photolysis (j = 1 to 10). To obtain an ideal fitting, we also made a small adjustment of $C_{0.0}$ to between 0.15 and 0.33 μM by changing R_{min} (0.35–0.367) in some cells (c3,c4,c7). The parameters thus obtained are shown in Table 1 and are represented by polygonal lines in Figures 5 to 7. Hill coefficients of ≥ 2 are necessary to fit the data for Purkinje cells (Figure 5) but not to fit those for chromaffin cells loaded with 5,5′-difluoro-BAPTA (Figure 7). The polygonal lines for improper values of n_H in Figures 5 and 7 are drawn by maintaining the ideal value of the total binding sites, $n_H[H]$, unaltered. Clear distinction from the optimal fitting indicates that our method is sufficiently sensitive to evaluate n_H between 1 and 3.

For repetitive depolarization experiments, the extent of Ca^{2+} influx, ΔC_T, was assumed to be the same for each depolarization pulse. With the analytical method, the value of ΔC_T was estimated so as to account for the value of [H] obtained for the same cell (c1, c3, c4, c8), or to fulfill $\beta_\Delta = 200$ μM at $C = 1$ μM in the cells in which DMNPE-4 was not introduced (c10, c11, c12, c13) (Figures 6C and 6D). After ΔC_T is determined, the plot of $\beta\Delta$ can be obtained from Equations 16 and 11, and its analytical fit is obtained by Equations 18 and 19.

The temporal changes in C can be described by

$$\frac{dC}{dt} = -\frac{dC_B(C)}{dt} - P(C - C_i) + I(t) \quad (20)$$

where P represents the pump rate (/s), C_r the resting [Ca^{2+}]$_i$, and $I(t)$ the Ca^{2+} influx at a given time (M/s). If we assume the rapid buffer approximation (Neher, 1998), where the kinetics of Ca^{2+} binding are so rapid that the buffers are equilibrated with Ca^{2+}, then

$$\frac{dC_B(C)}{dt} = \frac{dC_B(C)}{dC}\frac{dC}{dt} \quad (21)$$

and

$$(1 + \frac{dC_B(C)}{dC})\frac{dC}{dt} = -P(C - C_i) + I(t) \quad (22)$$

This relation indicates that the time constant, τ, for the decay in C depends on C as follows

$$\tau(C) = (1 + \kappa_L + \kappa_H(C)) / P \quad (23)$$

where $\kappa_H(C)$ is defined by Equation 4, and that the increment in $[Ca^{2+}]_i$ induced by a small influx of Ca^{2+} is reduced by the high-affinity Ca^{2+} buffer according to a supralinearity factor (S) given by

$$S(C) = (1 + \kappa_L + \kappa_H(C)) / (1 + \kappa_L) \quad (24)$$

The spatiotemporal distribution of C is described by a nonlinear cable equation (Zador and Koch, 1994) as follows

$$\tau(C) \frac{\partial C}{\partial t} = \lambda^2 (C) \frac{\partial^2 C}{\partial x^2} - (C - C_r) + I (x,t) / P \quad (25)$$

where λ is a length constant that depends on C as follows

$$\lambda^2 (C) = (D_{Ca} + \kappa_L D_L + \kappa_H (C) D_H) / P \quad (26)$$

and where D_{Ca}, D_H, and D_L are the diffusion coefficients ($\mu m^2/s$) of free Ca^{2+} and the high- and low-affinity buffers. The apparent diffusion coefficient of Ca^{2+} in the presence of the two buffers is Ca^{2+} dependent and given by

$$D_{app} (C) = \lambda^2 (C) / \tau(C) \quad (27)$$

The diffusion coefficients of the buffers were estimated by applying the cable equation to the somas of cells with a bipolar morphology (Figure 8A, inset). We approximate Ca^{2+} diffusion with a seven-compartment model oriented along the main somatic axis. Each compartment is 1 by 3 μm in size. Gradients of $[Ca^{2+}]_i$ orthogonal to the somatic axis were dissipated to a level below the resolution of our imaging system within 80 to 150 ms after the cessation of depolarization, unlike the case with chromaffin cells (Naraghi et al., 1998). The innermost compartment, S_6, was chosen so that $[Ca^{2+}]_i$ in S_6, $C_6(t)$, was almost identical to that $[C_7(t)]$ of the next compartment, S_7. We predicted $C_6(t)$ by assigning the actual time course of $[Ca^{2+}]_i$ in the outermost compartment, $C_0(t)$, and actual values of $C_1(0),..,C_6(0)$. The diameters of the soma along the compartments were increased by 0 to 15%. The effect of the change in diameter on diffusion was corrected for by estimating the relative diameter (d_i) of the soma at each compartment on the basis of the mean BTC fluorescence, and Ca^{2+} diffusion along the soma was simulated with the following six simultaneous ordinary differential equations:

$$(1 + \kappa_L + \kappa_H (C_i)) \frac{\partial C_i}{\partial t} = -P(C_i - C_r) \quad (28)$$
$$+ \sum_{J=0}^{3} D_j \left[\frac{d_{i-1}}{d_i} Cb_j (C_{i-1}) - \frac{d_{i-1} + d_{i+1}}{d_i} Cb_j (C_i) + \frac{d_{i+1}}{d_i} Cb_j (C_{i+1}) \right],$$
$$i = 1 ,..., 6$$

where $C_7(t) = C_6(t)$; D_0, D_1, D_2, and D_3 represent D_{Ca}, D_H, D_L, and D_{BTC}, respectively; and Cb_0, Cb_1, Cb_2, and Cb_3 are the concentrations of free calcium and of calcium bound to the high- and low-affinity Ca^{2+} buffers and to BTC, respectively. We assumed the standard buffer parameters ($[H] = 0.4$ mM, $K_H = 0.35$ μM, $n_H = 2$, and $\kappa_L = 100$) as well as a BTC concentration of 0.6 mM, with $K_{BTC} = 15$ μM, $D_{BTC} = 100$ $\mu m^2/s$, $D_{Ca} = 233$ $\mu m^2/s$, $P = 5/s$, and $C_r = 0.1$ μM. The values D_H and D_L were obtained so that the predicted $C_6(t)$ most closely resembles the actual time course. The simulation was performed with the "NDSolve" function of Mathematica 3.0 software (Wolfram Research).

The simulation experiments for nonlinear Ca^{2+} cable properties were performed with a 19-compartment model (Figures 9F and 9H). Calcium influx was applied to all compartments for the global input and to the middle compartment for the local input. We used the standard buffer parameters, with $D_L = 0$ and $P = 2000/s$. The Ca^{2+} transients induced by the global Ca^{2+} input are the same irrespective of D_H, whereas those induced by the local input are markedly reduced by diffusion.

Acknowledgments

We thank T. Kishimoto, M. Ogawa, and M. Osaka for technical assistance, as well as E. Neher, A. Konnerth, G. J. Augustine, and Y. Mori for helpful discussions. This work was supported by the Research for the Future program of the Japan Society for the Promotion of Science (JSPS); Grants-in-Aid from the Japanese Ministry of Education, Science, Sports, and Culture; a research grant from the Human Frontier Science Program; CREST (Core Research for Evolutional Science and Technology) of the Japan Science and Technology Corporation (JST); and the National Institutes of Health (GM53395).

Received August 18, 1999; revised August 31, 1999.

References

Ahmed, Z., and Connor, J.A. (1988). Calcium regulation by and buffer capacity of molluscan neurons during calcium transients. Cell Calcium *9*, 57–69.

Airaksinen, M.S., Eilers, J., Garaschuk, O., Thoenen, H., Konnerth, A., and Meyer, M. (1997a). Ataxia and altered dendritic calcium signaling in mice carrying a targeted null mutation of the calbindin D28k gene. Proc. Natl. Acad. Sci. USA *94*, 1488–1493.

Airaksinen, M.S., Thoenen, H., and Meyer, M. (1997b). Vulnerability of midbrain dopaminergic neurons in calbindin-D28k-deficient mice: lack of evidence for a neuroprotective role of endogenous calbindin in MPTP-treated and weaver mice. Eur. J. Neurosci. *9*, 120–127.

Allbritton, N.L., Meyer, T., and Stryer, L. (1992). Range of messenger action of calcium ion and inositol 1,4,5-trisphosphate. Science *258*, 1812–1815.

Al-Baldawi, N.F., and Abercrombie, R.F. (1995). Calcium diffusion coefficient in Myxicola axoplasm. Cell Calcium *17*, 422–430.

Arnold, D.B., and Heintz, N. (1997). A calcium responsive element that regulates expression of two calcium binding proteins in Purkinje cells. Proc. Natl. Acad. Sci. USA *94*, 8842–8847.

Baimbridge, K.G., Miller, J.J., and Parkes, C.O. (1982). Calcium-binding protein distribution in the rat brain. Brain Res. *239*, 519–525.

Baimbridge, K.G., Celio, M.R., and Rogers, J.H. (1992). Calcium-binding proteins in the nervous system. Trends Neurosci. *15*, 303–308.

Baker, P.F., and Schlaepfer, W.W. (1978). Uptake and binding of calcium by axoplasm isolated from giant axons of Loligo and Myxicola. J. Physiol. (Lond.) *276*, 103–125.

Berridge, M.J. (1993). Inositol trisphosphate and calcium signaling. Nature *361*, 315–325.

Calvet, M.C., Calvet, J., and Camacho-Garcia, R. (1985). The Purkinje cell dendritic tree: a computer-aided study of its development in the cat and in culture. Brain Res. *331*, 235–250.

Chard, P.S., Bleakman, D., Christakos, S., Fullmer, C.S., and Miller, R.J. (1993). Calcium buffering properties of calbindin D_{28k} and parvalbumin in rat sensory neurones. J. Physiol. (Lond.) *472*, 341–357.

Cheung, W.T., Richards, D.E., and Rogers, J.H. (1993). Calcium binding by chick calretinin and rat calbindin D28k synthesised in bacteria. Eur. J. Biochem. *215*, 401–410.

DelPrincipe, F., Egger, M., Ellis-Davies, G.C.R., and Niggli, E. (1999). Two-photon and UV-laser flash photolysis of the Ca^{2+} cage, dimethoxynitrophenyl-EGTA-4. Cell Calcium *25*, 85–91.

Eilers, J., Augustine, G.J., and Konnerth, A. (1995a). Subthreshold synaptic Ca^{2+} signaling in fine dendrites and spines of cerebellar Purkinje neurons. Nature *373*, 155–158.

Eilers, J., Callewaert, G., Armstrong, C., and Konnerth, A. (1995b). Calcium signaling in a narrow somatic submembrane shell during synaptic activity in cerebellar Purkinje neurons. Proc. Natl. Acad. Sci. USA *92*, 10272–10276.

Ekerot, C.F., and Kano, M. (1989). Stimulation parameters influencing climbing fibre induced long-term depression of parallel fibre synapses. Neurosci. Res. *6*, 264–268.

Ellis-Davies, G.C.R. (1998). Synthesis of photosensitive EGTA derivatives. Tetrahedron Lett. *39*, 953–956.

Falke, J.J., Drake, S.K., Hazard, A.L., and Peersen, O.B. (1994). Molecular tuning of ion binding to calcium signaling protein. Q. Rev. Biophys. *27*, 219–290.

Fierro, L., and Llano, I. (1996). High endogenous calcium buffering in Purkinje cells from rat cerebellar slices. J. Physiol. (Lond.) *496*, 617–625.

Fierro, L., DiPolo, R., and Llano, I. (1998). Intracellular calcium clearance in Purkinje cell somata from rat cerebellar slices. J. Physiol. (Lond.) *510*, 499–512.

Finch, E.A., and Augustine, G.J. (1998). Local calcium signaling by inositol-1,4,5-trisphosphate in Purkinje cell dendrites. Nature *396*, 753–756.

Gabso, M., Neher, E., and Spira, M.E. (1997). Low mobility of the Ca^{2+} buffers in axons of cultured Aplysia neurons. Neuron *18*, 473–481.

Hartell, N.A. (1996). Strong activation of parallel fibers produces localized calcium transients and a form of LTD that spreads to distant synapses. Neuron *16*, 601–610.

Hashimoto, T., Ishii, T., and Ohmori, H. (1996). Release of Ca^{2+} is the crucial step for the potentiation of IPSCs in the cultured cerebellar Purkinje cells of the rat. J. Physiol. (Lond.) *497*, 611–627.

Heizmann, C.W., and Braun, K. (1992). Changes in Ca^{2+}-binding proteins in human neurodegenerative disorders. Trends Neurosci. *15*, 259–264.

Helmchen, F., Imoto, K., and Sakmann, B. (1996). Ca^{2+} buffering and action potential-evoked Ca^{2+} signaling in dendrites of pyramidal neurons. Biophys. J. *70*, 1069–1081.

Hirano, T. (1990). Effects of postsynaptic depolarization in the induction of synaptic depression between a granule cell and a Purkinje cell in rat cerebellar culture. Neurosci. Lett. *119*, 145–147.

Hirano, T., and Ohmori, H. (1986). Voltage-gated and synaptic currents in rat Purkinje cells in dissociated cell cultures. Proc. Natl. Acad. Sci. USA *83*, 1945–1949.

Hirose, K., Kadowaki, S., and Iino, M. (1998). Allosteric regulation by cytoplasmic Ca^{2+} and IP_3 of the gating of IP_3 receptors in permeabilized guinea-pig vascular smooth muscle cells. J. Physiol. (Lond.) *506*, 407–414.

Hockberger, P.E., Tseng, H.Y., and Connor, J.A. (1989). Fura-2 measurements of cultured rat Purkinje neurons show dendritic localization of Ca^{2+} influx. J. Neurosci. *9*, 2272–2284.

Hounsgaard, J., and Midtgaard, J. (1989). Synaptic control of excitability in turtle cerebellar Purkinje cells. J. Physiol. (Lond.) *409*, 157–170.

Ito, K., Miyashita, Y., and Kasai, H. (1997). Micromolar and submicromolar Ca^{2+} spikes regulating distinct cellular functions in pancreatic acinar cells. EMBO J. *16*, 242–251.

Ito, K., Miyashita, Y., and Kasai, H. (1999). Kinetic control of multiple forms of Ca^{2+} spikes by inositol trisphosphate in pancreatic acinar cells. J. Cell Biol. *146*, 405–414.

Ito, M., Sakurai, M., and Tongroach, P. (1982). Climbing fibre induced depression of both mossy fibre responsiveness and glutamate sensitivity of cerebellar Purkinje cells. J. Physiol. (Lond.) *324*, 113–134.

Kaftan, E.J., Ehrlich, B.E., and Watras, J. (1997). Inositol 1,4,5-trisphosphate ($InsP_3$) and calcium interact to increase the dynamic range of $InsP_3$ receptor-dependent calcium signaling. J. Gen. Physiol. *110*, 529–538.

Kano, M., Rexhausen, U., Dreessen, J., and Konnerth, A. (1992). Synaptic excitation produces a long-lasting rebound potentiation of inhibitory synaptic signals in cerebellar Purkinje cells. Nature *356*, 601–604.

Kano, M., Garaschuk, O., Verkhratsky, A., and Konnerth, A. (1995). Ryanodine receptor-mediated intracellular calcium release in rat cerebellar Purkinje neurones. J. Physiol. (Lond.) *487*, 1–16.

Kasai, H. (1993). Cytosolic Ca^{2+} gradients, Ca^{2+} binding proteins and synaptic plasticity. Neurosci. Res. *16*, 1–7.

Kasai, H., and Petersen, O.H. (1994). Spatial dynamics of second messengers: IP_3 and cAMP as long-range and associative messengers. Trends Neurosci. *17*, 95–101.

Kasai, H., and Takahashi, N. (1999). Multiple kinetic components and the Ca^{2+} requirements of exocytosis. Philos. Trans. R. Soc. Lond. B Biol. Sci. *354*, 331–335.

Kobayashi, K., and Tachibana, M. (1995). Ca^{2+} regulation in the presynaptic terminals of goldfish retinal bipolar cells. J. Physiol. (Lond.) *483*, 79–94.

Konnerth, A., Dreessen, J., and Augustine, G.J. (1992). Brief dendritic calcium signals initiate long-lasting synaptic depression in cerebellar Purkinje cells. Proc. Natl. Acad. Sci. USA *89*, 7051–7055.

Kosaka, T., Kosaka, K., Nakayama, T., Hunziker, W., and Heizmann, C.W. (1993). Axons and axon terminals of cerebellar Purkinje cells and basket cells have higher levels of parvalbumin immunoreactivity than somata and dendrites: quantitative analysis by immunogold labeling. Exp. Brain Res. *93*, 483–491.

Lev-Ram, V., Jiang, T., Wood, J., Lawrence, D.S., and Tsien, R.Y. (1997). Synergies and coincidence requirements between NO, cGMP, and Ca^{2+} in the induction of cerebellar long-term depression. Neuron *18*, 1025–1038.

Linden, D. (1999). The return of the spike: postsynaptic action potentials and the induction of LTP and LTD. Neuron *22*, 661–666.

Linden, D.J., Dickinson, M.H., Smeyne, M., and Connor, J.A. (1991). A long-term depression of AMPA currents in cultured cerebellar Purkinje neurons. Neuron *7*, 81–89.

Llano, I., Leresche, N., and Marty, A. (1991). Calcium entry increases the sensitivity of cerebellar Purkinje cells to applied GABA and decreases inhibitory synaptic currents. Neuron *6*, 565–574.

Llano, I., DiPolo, R., and Marty, A. (1994). Calcium-induced calcium release in cerebellar Purkinje cells. Neuron *12*, 663–673.

Markram, H., Roth, A., and Helmchen, F. (1998). Competitive calcium binding: implications for dendritic calcium signaling. J. Computational Neurosci. *5*, 331–348.

Mattson, M.P., Rychlik, B., Chu, C., and Christakos, S. (1991). Evidence for calcium-reducing and excito-protective roles for the calcium-binding protein calbindin-D28k in cultured hippocampal neurons. Neuron *6*, 41–51.

Mintz, I.M., Venema, V.J., Swiderek, K.M., Lee, T.D., Bean, B.P., and Adams, M.E. (1992). P-type calcium channels blocked by the spider toxin omega-Aga-IVA. Nature *355*, 827–829.

Miyakawa, H., Lev-Ram, V., Lasser-Ross, N., and Ross, W.N. (1992). Calcium transients evoked by climbing fiber and parallel fiber synaptic inputs in guinea pig cerebellar Purkinje neurons. J. Neurophysiol. *68*, 1178–1189.

Molinari, S., Battini, R., Ferrari, S., Pozzi, L., Killcross, A.S., Robbins, T.W., Jouvenceau, A., Billard, J.M., Dutar, P., Lamour, Y., et al. (1996). Deficits in memory and hippocampal long-term potentiation in mice with reduced calbindin D_{28K} expression. Proc. Natl. Acad. Sci. USA *93*, 8028–8033.

Muller, T.H., Partridge, L.D., and Swandulla, D. (1993). Calcium buffering in bursting Helix pacemaker neurons. Pflugers Arch. *425*, 499–505.

Naraghi, M., Muller, T.H., and Neher, E. (1998). Two-dimensional determination of the cellular Ca^{2+} binding in bovine chromaffin cells. Biophys. J. *75*, 1635–1647.

Neher, E. (1995). The use of fura-2 for estimating Ca buffers and Ca fluxes. Neuropharmacology *34*, 1423–1442.

Neher, E. (1998). Usefulness and limitations of linear approximations to the understanding of Ca^{++} signals. Cell Calcium *24*, 345–357.

Neher, E., and Augustine, G.J. (1992). Calcium gradients and buffers in bovine chromaffin cells. J. Physiol. (Lond.) *450*, 273–301.

Neher, E., and Zucker, R.S. (1993). Multiple calcium-dependent processes related to secretion in bovine chromaffin cells. Neuron *10*, 21–30.

Ninomiya, Y., Kishimoto, T., Yamazawa, T., Ikeda, H., Miyashita, Y., and Kasai, H. (1997). Kinetic diversity in the fusion of exocytotic vesicles. EMBO J. *16*, 929–934.

Push, M., and Neher, E. (1988). Rates of diffusional exchange between small cells and a measuring patch pipette. Pflugers Arch. *411*, 204–211.

Roberts, W.M. (1993). Spatial calcium buffering in saccular hair cells. Nature *363*, 74–76.

Sakurai, M. (1990). Calcium is an intracellular mediator of the climbing fiber in induction of cerebellar long-term depression. Proc. Natl. Acad. Sci. USA *87*, 3383–3385.

Schneggenburger, R., Zhou, Z., Konnerth, A., and Neher, E. (1993). Fractional contribution of calcium to the cation current through glutamate receptor channels. Neuron *11*, 133–143.

Schwiening, C.J., and Thomas, R.C. (1996). Relationship between intracellular calcium and its muffling measured by calcium iontophoresis in snail neurones. J. Physiol. *491*, 621–633.

Shibuki, K., and Okada, D. (1991). Endogenous nitric oxide release

required for long-term synaptic depression in the cerebellum. Nature *349*, 326–328.

Sobel, E.C., and Tank, D.W. (1999). In vivo Ca^{2+} dynamics in a cricket auditory neuron: an example of chemical computation. Science *263*, 823–825.

Takechi, H., Eilers, J., and Konnerth, A. (1998). A new class of synaptic response involving calcium release in dendritic spines. Nature *396*, 757–760.

Tank, D.W., Sugimori, M., Connor, J.A., and Llinas, R.R. (1988). Spatially resolved calcium dynamics of mammalian Purkinje cells in cerebellar slice. Science *242*, 773–777.

Tatsumi, H., and Katayama, Y. (1993). Regulation of the intracellular free calcium concentration in acutely dissociated neurones from rat nucleus basalis. J. Physiol. (Lond.) *464*, 165–181.

Tse, A., Tse, F.W., and Hille, B. (1994). Calcium homeostasis in identified rat gonadotrophs. J. Physiol. (Lond.) *477*, 511–525.

Wang, S.S., and Augustine, G.J. (1995). Confocal imaging and local photolysis of caged compounds: dual probes of synaptic function. Neuron *15*, 755–760.

Xu, T., Naraghi, M., Kang, H., and Neher, E. (1997). Kinetic studies of Ca^{2+} binding and Ca^{2+} clearance in the cytosol of adrenal chromaffin cells. Biophys. J. *73*, 532–545.

Yamakuni, T., Kuwano, R., Odani, S., Miki, N., Yamaguchi, K., and Takahashi, Y. (1987). Molecular cloning of cDNA to mRNA for a cerebellar spot 35 protein. J. Neurochem. *48*, 1590–1596.

Zador, A., and Koch, C. (1994). Linearized models of calcium dynamics: formal equivalence to the cable equation. J. Neurosci. *14*, 4705–4715.

Zhou, Z., and Neher, E. (1993). Mobile and immobile calcium buffers in bovine adrenal chromaffin cells. J. Physiol. (Lond.) *469*, 245–273.